Electron paramagnetic resonance and optical spectra of Cr^{3+}-doped $YAlO_3$

1993 J. Phys.: Condens. Matter 5 8097

(http://iopscience.iop.org/0953-8984/5/43/021)

J. Phys.: Condens. Matter 5 (1993) 8097–8104. Printed in the UK

Electron paramagnetic resonance and optical spectra of Cr^{3+}-doped $YAlO_3$

M Yamaga†, H Takeuchi‡, T P J Han§ and B Henderson§

† Department of Physics, Faculty of General Education, Gifu University, Gifu 501-11, Japan

‡ Department of Physics, College of General Education, Nagoya University, Nagoya 464-01, Japan

§ Department of Physics and Applied Physics, University of Strathclyde, Glasgow G4 0NG, UK

Received 26 July 1993

Abstract. This paper reports electron paramagnetic resonance (EPR) measurements of Cr^{3+} ions in $YAlO_3$ (YAP) at 1.6 K and room temperature along with their optical absorption and luminescence spectra. The polarization of the excitation spectrum of the Cr^{3+} luminescence has also been measured. The EPR spectrum is ascribed to substitutional Cr^{3+} ions at Al^{3+} sites. The spin-Hamiltonian parameters determined from the EPR spectrum of Cr^{3+} ions in nearly orthorhombic sites in YAP are $g_x = 1.981$, $g_y = 1.981$, $g_z = 1.981$, $b_2^0 = +445 \times 10^{-4}$ cm^{-1} and $b_2^2 = -278 \times 10^{-4}$ cm^{-1}. The anisotropy of the Cr^{3+} EPR spectrum is discussed in terms of the electrostatic potential of the surrounding O^{2-} and Y^{3+} ions in YAP crystals and is compared with that of Ti^{3+} ions in the same host crystal.

1. Introduction

Yttrium aluminium perovskite, $YAlO_3$ (YAP), is a host crystal that supports laser action when containing rare-earth ions and transition-metal ions [1]. The broad-band absorption spectra of Cr^{3+} in YAP are due to $^4A_2 \rightarrow {}^4T_2$ and $^4A_2 \rightarrow {}^4T_1$ transitions [2]. The luminescence from Cr^{3+} ions in YAP consists of the sharp R line and its phonon sidebands due to the $^2E \rightarrow {}^4A_2$ transition [3]. Recently, Ti^{3+}-doped YAP [4–6] has attracted considerable interest in view of its potential as a solid-state laser material operating at shorter wavelengths than Ti^{3+}-doped Al_2O_3.

The polarization of the optical absorption and luminescence spectra of transition-metal ions such as Cr^{3+} and Ti^{3+} depends strongly on the structure of the host YAP crystal in which the Al^{3+} ions occupy sites that are slightly distorted from perfectly orthorhombic symmetry [7, 8]. In order to examine the surroundings of Cr^{3+} and Ti^{3+} in YAP, EPR measurements were carried out at room temperature and 1.6 K. This paper discusses the relationship between the YAP crystal structure and the spin-Hamiltonian parameters of the measured g tensor and fine-structure tensor of the paramagnetic Cr^{3+} ions. The experimental results for Cr^{3+} in YAP are also compared with those of Ti^{3+} in the same host crystal [9].

2. Crystal structure of $YAlO_3$

The slightly distorted perovskite structure of YAP crystals belongs to the space group D_{2h}^{16} ($Pbnm$). Early x-ray diffraction studies were reported by Geller and Wood [7].

0953-8984/93/438097+08$07.50

Subsequently, the crystallographic parameters were refined by Diehl and Brandt [8]. A projection of the unit cell on to the c plane of the crystal is shown in figure 1: four structurally equivalent Al^{3+} sites are denoted as I, II, III and IV. In YAP Cr^{3+} ion impurities substitute for Al^{3+} ions at the centre of a distorted octahedral arrangement of O^{2-} ligand ions.

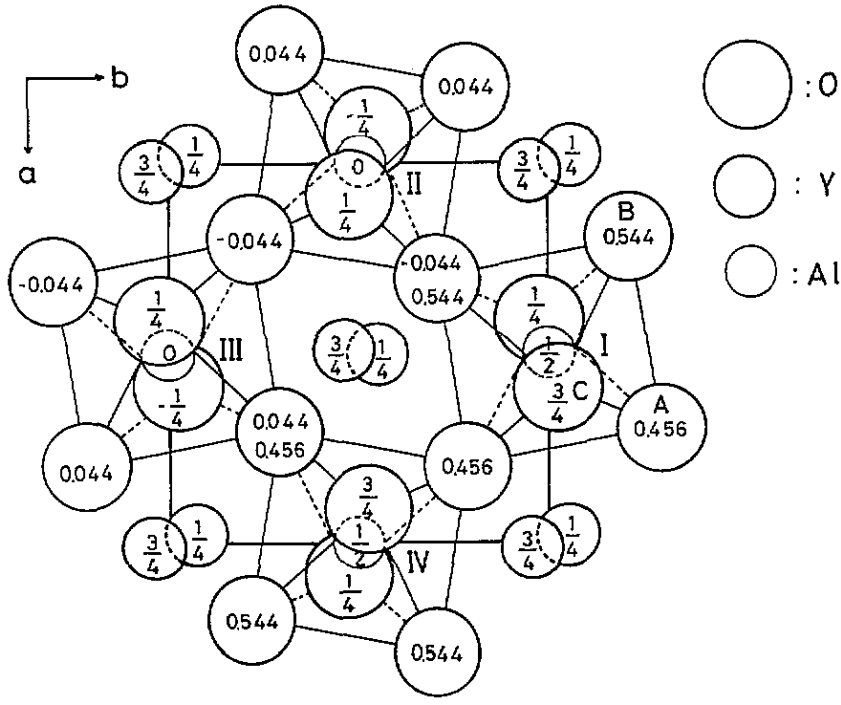

Figure 1. Orthogonal projection of a unit cell of YAP on to the (001) plane.

3. Experimental procedure and results

Single crystals were grown by the Czochralski method from melts containing 0.1 mol% Cr_2O_3. Samples with dimensions of $\sim 4 \times 4 \times 5$ mm^3 were cut from boules, the cut faces being normal to the [100], [010], and [001] directions associated with the a, b, and c axes of the crystal as shown in figure 1. The EPR measurements were made at room temperature using an X-band ($\nu \simeq 9.4$ GHz) EPR spectrometer with 100 kHz field modulation and at 1.6 K using a Q-band ($\nu \simeq 34$ GHz) spectrometer. The sample was rotated using a two-axis goniometer in a cylindrical X-band cavity operating in the TE_{011} mode. Numerical calculations for the matrix diagonalization of the spin Hamiltonian were performed using the computer at the computation centre of Nagoya University. Emission and excitation spectra of the Cr^{3+} ions were measured at room temperature using a Hitachi MPF4 fluorescence spectrometer. The measurements of the temperature dependence of the emission spectrum were made from samples enclosed in the vacuum space of a cryorefrigerator capable of working at temperatures in the range 10–300 K.

3.1. EPR measurements

The EPR spectra measured at X band ($\nu \simeq 9.4$ GHz) at 300 K and Q band ($\nu \simeq 34$ GHz) at 1.6 K are equivalent, after making due allowance for the different frequencies. Figure 2 shows the typical X-band EPR spectra, consisting of three lines, observed at room temperature with magnetic fields parallel to the a, b, and c axes. Angular variations of EPR spectra were measured with the magnetic field in the (001), (100), and (010) planes. An orientation plot for magnetic field directions in the (001) plane is shown in figure 3, in which the open circles denote the observed resonant fields. Each line splits into two branches with the magnetic field in the (001), (100), and (010) planes. These results indicate that the EPR signals are due to Cr^{3+} ($S = \frac{3}{2}$) ions at four structurally identically Al^{3+} sites, differently orientated with respect to the axes of the crystal, which become equivalent when the applied field is parallel to the a, b, or c axes.

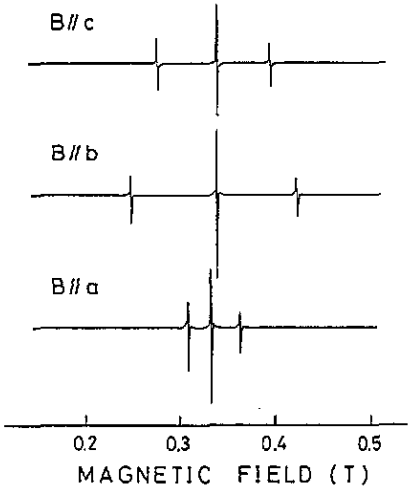

Figure 2. Typical X-band EPR spectra of Cr^{3+} observed at room temperature with $B \parallel a$, b, and c axes. The microwave frequency 9.36 GHz.

The angular variations of the EPR spectra may be fitted to the spin Hamiltonian appropriate to orthorhombic symmetry

$$H = g_x \mu_B S_x B_x + g_y \mu_B S_y B_y + g_z \mu_B S_z B_z + \tfrac{1}{3}(b_2^0 O_2^0 + b_2^2 O_2^2) \qquad (1)$$

where $S = \frac{3}{2}$, μ_B is the Bohr magneton and O_n^m are the Stevens operators [10]. The principal x, y, and z axes are selected so as to satisfy the condition that $|b_2^2/b_2^0| < 1$; the z axis is defined as the magnetic field direction in which fine structure splitting is maximal. The magnetic field directions were accurately set to be parallel to the three orthogonal principal axes using the two-axis goniometer. The polar angles θ_k and ϕ_k ($k = x, y, z$) for the principal x, y, and z axes are defined with respect to the abc-coordinate system, as shown in figure 4. The spin-Hamiltonian parameters are obtained by the matrix diagonalization method using the resonant fields and the polar angles of the three principal-axis directions. The results are summarized in table 1. The previously reported data for Cr^{3+} in YAP [11], as well as those for Fe^{3+} in YAP [12] and Ti^{3+} in YAP [9] are also listed in table 1 for comparison. The full curves in figure 3, calculated using equation (1) with the spin-Hamiltonian parameters and the polar angles of the principal axes in table 1, are in good agreement with the experimental points.

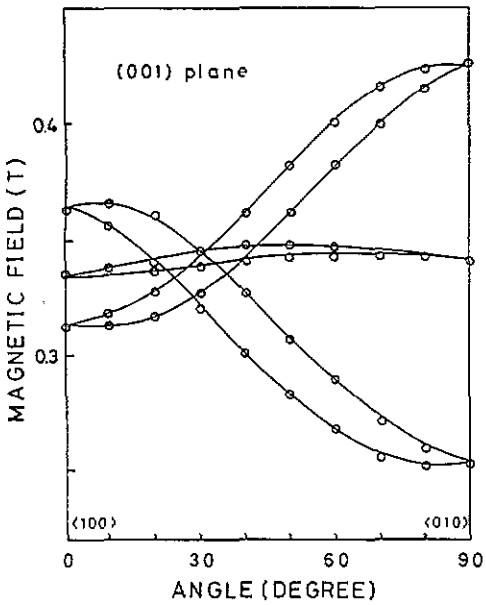

Figure 3. Angular dependence of the X-band EPR spectra observed at room temperature with the magnetic field in the (001) plane. The frequency is 9.46 GHz. Full curves are calculated using equation (1) and the spin-Hamiltonian parameters in table 1.

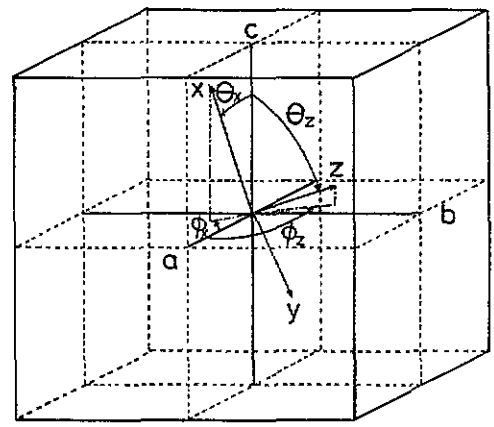

Figure 4. Definition of the principal axes x, y, z and their polar angles of Cr^{3+} with respect to the *abc*-coordinate system.

Table 1. The spin-Hamiltonian parameters and polar angles of principal axis directions of Cr^{3+} ions. Units are 10^{-4} cm^{-1} for b_2^m ($m = 0, 2$) and ° for polar angles.

Crystal	g_x	g_y	g_z	b_2^0	b_2^2	θ_x	ϕ_x	θ_z	ϕ_z	Reference
Cr^{3+}:YAP	1.981(1)	1.981(1)	1.981(1)	+445(2)	−278(2)	26(1)	−20(1)	75(1)	97(1)	This work
Cr^{3+}:YAP	1.98	1.98	1.98	−410	−300	25	—	79	96	[11]
Fe^{3+}:YAP	2.00	2.00	2.00	−1352	+840	38	158	90	68	[12]
Ti^{3+}:YAP	1.975	1.850	1.945	—	—	117	31	30	60	[9]

The purpose of measuring the Q-band EPR spectrum at 1.6 K was to reveal the depopulation effects between the different M_s levels, thereby determining the sign of the ground-state splitting. In this EPR spectrum, the high-field component of the fine structure was more intense than the low-field line when the magnetic field was applied near the z axis. This confirms the positive sign of b_2^0. This is in contrast to the b_2^0 given in [11] and shown in table 1.

The angular variation of the EPR spectra indicates that each of the two branches in figure 2 corresponds to the type-I and -III octahedra or the type-II and -IV octahedra where the type-I and -III (-II and -IV) octahedra are equivalent for the magnetic field in the (001) plane. However, the EPR results cannot identify the particular octahedron responsible for the principal axis directions given in table 1. This point is further discussed in the next section.

The EPR results observed at room temperature and 1.6 K show the existence of isolated Cr^{3+} ions in the crystal. Fairly weak signals due to Gd^{3+} and Fe^{3+} ions and an unknown centre, about two orders of magnitude weaker in intensity than those due to the isolated

Cr^{3+} ions, were observed. The angular variation of the unknown spectrum indicates that the total spin $S \geqslant 1$. It is possible that the unknown spectrum is due to pairs of Cr^{3+}, if the super-exchange coupling J is assumed to be fairly small ($J < 1\ cm^{-1}$). However, the identification of the pair requires further EPR measurement.

3.2. Optical measurements

The present investigation has shown that the optical absorption spectrum of Cr^{3+}: YAP samples at room temperature consists of two broad bands with peaks of 410 nm and 520 nm. An earlier report by Weber and Varitimos [3] placed the optical absorption peaks at 410 nm and 555 nm. At room temperature the emission spectrum of Cr^{3+} in YAP excited at $\lambda = 565$ nm, figure 5, shows the strong R line characteristic of Cr^{3+} ions in strong crystal-field sites, accompanied by the Stokes' shifted vibronic sideband at longer wavelengths and the anti-Stokes' sidebands at shorter wavelengths. As the temperature is reduced down to 10 K, the intensity of the anti-Stokes' sideband decreases to zero and the linewidths of the R line and its sidebands are narrowed.

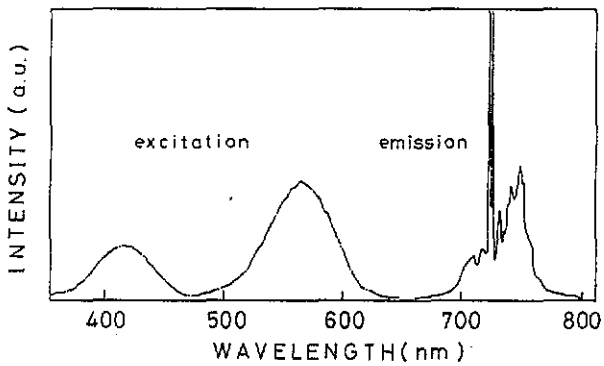

Figure 5. Emission and excitation spectra observed in Cr^{3+}:YAP at room temperature.

The left-hand side of figure 5 shows an excitation spectrum of the R line: the monochromator in the excitation channel of the spectrometer is scanned through the radiation spectrum of a Xe lamp, while the detecting monochromator is set at the R-line wavelength of 735 nm. Thus the excitation spectrum measures the intensity of R-line luminescence as a function of the wavelength of radiation absorbed by Cr^{3+} ions in the crystal. In consequence, the excitation peaks at 415 nm and 565 nm are associated with the $^4A_2 \rightarrow {}^4T_1$ and $^4A_2 \rightarrow {}^4T_2$ transitions, respectively. The excitation spectrum of the R line should correspond approximately to the absorption spectrum of Cr^{3+} ions in strong-crystal-field sites. The excitation peaks are close to the peaks in the absorption spectrum of isolated Cr^{3+} ions reported by Weber and Varitimos [3]. The reason the difference between the presently observed absorption spectrum and the excitation spectra in figure 5 is not clear. The observed absorption peaks at 410 nm and 520 nm are not due to the isolated Cr^{3+} ions, but may be due to complexes of Cr^{3+} ions.

The excitation band corresponding to the $^4A_2 \rightarrow {}^4T_2$ transition is polarized along the a, b, and c axes of the crystal and has peaks at 565 nm, 569 nm, and 565 nm, respectively, the peak of the b-polarized band being shifted to longer wavelength.

4. Discussion

The polar angles of the principal z axis of Cr^{3+} ions in YAP were determined from the angular variation of the EPR spectra to be $(\theta_z, \phi_z) = (75°, 97°)$, as shown in table 1. Here we consider which of the four octahedra in figure 1 corresponds to the octahedron with this principal z axis. The distances between a central Al^{3+} ion and the O^{2-} ligand ions in YAP are 1.911 Å, 1.921 Å, and 1.901 Å for the ligands A, B, and C of the type-I octahedron shown in figure 1. Apparently the octahedron is compressed along the c axis and stretched along the b axis. The observed z axis is not coincident with any one of the ligand directions, but is displaced by 75° from the c axis of the crystal. Furthermore, the projection of the z axis on the ab plane is displaced by 7° from the b axis towards the negative a axis. Such a crystal-field symmetry is not produced by the six nearest-neighbour O^{2-} ligand ions alone, but requires contributions to the crystal field from the eight second-nearest-neighbour Y^{3+} ions.

It is difficult to apply crystal-field theory to this problem because of the slightly distorted structure of YAP crystals. In order to determine the profile of the crystal field at the Cr^{3+} ion position, produced by the six nearest-neighbour O^{2-} ligand ions and the eight second-neighbour Y^{3+} ions, the counter maps of the electrostatic potential have been calculated regarding the O^{2-} and Y^{3+} ions as point charges. The crystal field is determined by the gradient of the electrostatic potential. The direction of the maximal positive gradient calculated for the type-I octahedron is displaced by 80° from the c axis towards the b axis and is close to the observed polar angle of the z axis. This qualitatively reflects the fact that Y^{3+} ions are displaced towards the b axis with respect to each other as shown in figure 1. Thus, the Cr^{3+} site that has the polar angles given in table 1 corresponds to the type-I octahedron.

Similar results were observed for Ti^{3+} ions in YAP [9]. The principal z axis of Ti^{3+}, being declined by some 15° from the ligand C direction in the type-I octahedron towards the b axis, is different from that of Cr^{3+} ions. We consider why the z axis of Cr^{3+} in YAP is different from that of Ti^{3+}. The ground state of Ti^{3+}, defined as $^2T_2$ in octahedral symmetry and shown in figure 6(b), is an orbitally degenerate triplet state. The Jahn–Teller effect lifts the degeneracy. As figure 6(b) shows the lowest state of the $^2T_2$ ground state is the orbital singlet $^2B_2$ when the octahedron is compressed along one of the ligand directions, whereas when the octahedron is stretched the orbital doublet ^2E is lowest. The distance of Al^{3+}–O^{2-}(C) in the type-I octahedron in figure 1 is the shortest. Assuming that the Jahn–Teller effect stabilizes an octahedron compressed along one of the ligand directions, the compression will be enhanced by an axial crystal field parallel to the Ti^{3+}–O^{2-}(C) direction. Then, the Ti^{3+}–O^{2-}(C) direction forms the z axis. In contrast, the ground state of Cr^{3+} ions is $^4A_2$, which is not perturbed by the Jahn–Teller effect because it is an orbital singlet. As the observed z axis of Cr^{3+} at the type-I octahedron is close to the b axis, the orthorhombic crystal field along the b axis may be stronger than the other two components. The difference in the principal z axes of Cr^{3+} and Ti^{3+} ions may then be caused by the absence or presence of the Jahn–Teller effect.

Next, we consider the relation between the fine structure and the crystal-field symmetry. The fine-structure term is written as

$$D_x S_x^2 + D_y S_y^2 + D_z S_z^2.$$

This term rewritten in the form of the spin Hamiltonian given in equation (1) uses

$$D_x = -\tfrac{1}{3}(b_2^0 - b_2^2) \qquad D_y = -\tfrac{1}{3}(b_2^0 + b_2^2) \qquad D_z = \tfrac{2}{3}b_2^0. \tag{2}$$

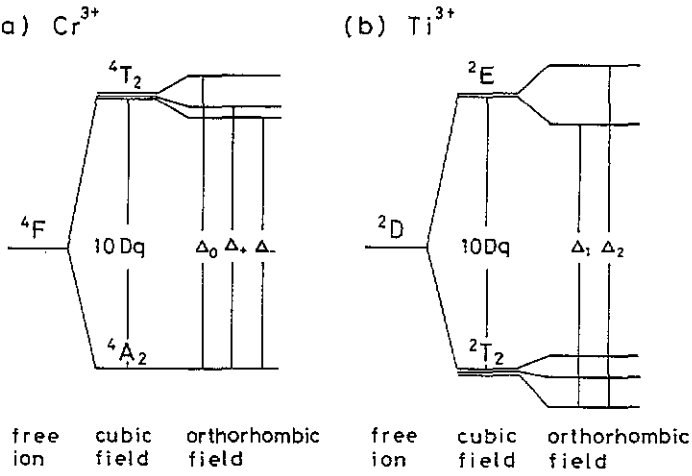

Figure 6. Schematical energy levels of (*a*) Cr^{3+} and (*b*) Ti^{3+} in YAP with orthorhombic symmetry.

Using the experimental values of b_2^0 and b_2^2 listed in table 1, we obtain $D_x = -241 \times 10^{-4}$ cm^{-1}, $D_y = -56 \times 10^4$ cm^{-1}, and $D_z = 297 \times 10^4$ cm^{-1}. The distance between the central ion and the O^{2-} ligand ions is shortest for the O C of the type-I octahedron in figure 1, so that the surrounding negative charge is densest about the x axis, being close to the crystalline c axis. This is consistent with the negative value of D_x. In contrast, D_z is positive. This indicates the distribution of some positive charge about the z axis, which is close to the crystalline b axis. As can be seen from figure 1, a structural phase transition of the perovskite-type crystal YAP occurs. One of the Y^{3+} ions along the b axis becomes very close to the central Cr^{3+} ion, whereas Y^{3+} ions along the a axis do not change their distance from the central ion so much. Roughly speaking, the electrostatic potential at the central ion from some near-neighbour ion is proportional to Ze/R, where R is the distance to the central ion and Ze is the charge on the relevant ion. The ratio of potentials from one Y^{3+} ion to that from one O^{2-} ion is about $\sqrt{3}/2$. So, the distortion from cubic symmetry of the first Y^{3+} shell may contribute significantly to the fine-structure splitting of the Cr^{3+} ion. It might be said that in the present Cr^{3+} centre in YAP the negative charge distribution due to compression along the c axis and the positive charge distribution due to the closest Y^{3+} ion along the b axis have almost the same magnitude ($|D_x| \simeq |D_z|$, and $|D_y| \simeq 0$).

The values of g factors and fine structure can be estimated from the degree of the orthorhombic distortion, because they are determined by the spin–orbit admixture of the $^4T_2$ excited state of Cr^{3+}. The g factors and fine-structure parameters of Cr^{3+} with low symmetry, for example, orthorhombic or monoclinic symmetry, were discussed by Pilbrow and Wood [13]. According to their theory, the g values are

$$g_x = 2 - 8\lambda/\Delta_- \qquad g_y = 2 - 8\lambda/\Delta_+ \qquad g_z = 2 - 8\lambda/\Delta_0 \tag{3}$$

where $\lambda = k\zeta/3$ (ζ is the one-electron spin–orbit constant and k the orbital reduction factor) and Δ_-, Δ_+, and Δ_0 are separation energies between three orbital levels of the $^4T_2$ excited states split by an orthorhombic distortion and a level of the $^4A_2$ ground state as shown in figure 6(*a*). The fine-structure parameters are given by

$$b_2^0 \equiv D = -2\lambda^2(2/\Delta_0 - 1/\Delta_+ - 1/\Delta_-) \tag{4}$$

$$b_2^2 \equiv 3E = 6\lambda^2(1/\Delta_+ - 1/\Delta_-). \tag{5}$$

The peak energies of the polarized excitation spectra due to the $^4A_2 \rightarrow {}^4T_2$ transition are used to estimate the values of Δ_0, Δ_+, and Δ_- as 17 700 cm^{-1}, 17 570 cm^{-1}, and 17 570 cm^{-1}, respectively. The spin–orbit coupling λ is obtained as 46 cm^{-1} from equation (3) and the measured values of Δ_0, Δ_+, and Δ_-. The value of b_2^0 is calculated to be 420×10^4 cm^{-1} using equation (4) with the above values of Δ_0, Δ_+, and Δ_-, and $\lambda = 50$ cm^{-1}. The calculated value is in good agreement with the observed value $b_2^0 = 445 \times 10^{-4}$ cm^{-1}. On the other hand, the separation of Δ_+ and Δ_- could not be observed by the polarization measurement so that the value of b_2^2 could not be estimated.

5. Conclusions

YAP has a slightly distorted perovskite structure with orthorhombic symmetry. The anisotropy of the crystal structure was discussed in terms of EPR measurements of Cr^{3+} ions replacing Al^{3+} in YAP. The Cr^{3+} ion is surrounded by six octahedral O^{2-} ion ligands. The observed principal axes of the Cr^{3+} complex, $(\theta_x, \phi_x) = (26°, -20°)$, $(\theta_y, \phi_y) = (112°, 13°)$, and $(\theta_z, \phi_z) = (75°, 97°)$ are not coincident with the O^{2-} ligand directions. This fact indicates that the crystal field of the Cr^{3+} ion is produced by the nearest-neighbour O^{2-} ligand ions of the Cr^{3+} ion and the second-nearest-neighbour Y^{3+} ions. The observed fine-structure parameter b_2^0 is in agreement with that calculated in terms of mixing of the $^4T_2$ excited orbital states into the $^4A_2$ ground state through spin–orbit interaction. The energy levels of the $^4T_2$ excited state split in the orthorhombic symmetry were obtained from the peak energies of the polarized excitation spectra.

Acknowledgments

This work was supported in part by a Grant in Aid for Scientific Research from the Ministry of Education, Science and Culture (03650032). One of the authors (M Yamaga) is indebted to the University of Strathclyde, the British Council, and the Daiwa Anglo-Japanese foundation for financial support.

References

[1] Kaminskii A A 1990 *Laser Crystals* (Berlin: Springer)
[2] Bass M and Weber M J 1970 *Appl. Phys. Lett.* **17** 395
[3] Weber M J and Varitimos T E 1974 *J. Appl. Phys.* **45** 810
[4] Schepler K L 1986 *Tunable Solid State Lasers II* ed A B Budgor, L Esterowitz and L G DeShazer (Berlin: Springer) pp 235–9
[5] Wegner T, Petermann K 1989 *Appl. Phys.* B **49** 275
[6] Yamaga M, Henderson B, O'Donnell K P, Rasheed F, Gao Y and Cockayne B 1991 *Appl. Phys.* B **52** 225
[7] Geller S and Wood E A 1956 *Acta Crystallogr.* **9** 563
[8] Diehl R and Brandt G 1975 *Mater. Res. Bull.* **10** 85
[9] Yamaga M, Yosida T, Henderson B, O'Donnell K P and Date M 1992 *J. Phys.: Condens. Matter* **4** 7285
[10] Abragam A and Bleaney B 1970 *Electron Paramagnetic Resonance of Transition Ions* (Oxford: Clarendon) ch 7, 10
[11] Pinto A and Sherman N Z 1972 *J. Magn. Reson.* **6** 422
[12] White R L, Hermann G F, Carson J W and Mandel M 1964 *Phys. Rev.* A **136** 231
[13] Pilbrow J R 1990 *Transition Ion Electron Paramagnetic Resonance* (Oxford: Clarendon) ch 3, 5